Published in final edited form as:
Inhal Toxicol. 2009 July ; 21(Suppl 1): 123–130. doi:10.1080/08958370902942582.

Effect of cerium oxide nanoparticles on inflammation in vascular endothelial cells

Andrea Gojova[1], **Jun-Tae Lee**[1], **Heejung S. Jung**[2], **Bing Guo**[3], **Abdul I. Barakat**[1], and **Ian M. Kennedy**[1]

[1] Department of Mechanical and Aeronautical Engineering, University of California, Davis, California

[2] Department of Mechanical Engineering, University of California, Riverside, California, USA

[3] Department of Mechanical Engineering, Texas A&M University, College Station, Texas, USA

Abstract

Because vascular endothelial cell inflammation is critical in the development of cardiovascular pathology, we hypothesized that direct exposure of human aortic endothelial cells (HAECs) to ultrafine particles induces an inflammatory response. To test the hypothesis, we incubated HAECs for 4 h with different concentrations (0.001–50 μg/ml) of CeO_2 nanoparticles and subsequently measured mRNA levels of the three inflammatory markers intercellular adhesion molecule 1 (ICAM-1), interleukin (IL)-8, and monocyte chemotactic protein (MCP-1) using real-time polymerase chain reaction (PCR). Ceria nanoparticles caused very little inflammatory response in HAECs, even at the highest dose. This material is apparently rather benign in comparison with Y_2O_3 and ZnO nanoparticles that we have studied previously. These results suggest that inflammation in HAECs following acute exposure to metal oxide nanoparticles depends strongly on particle composition.

Keywords

Ceria; nanoparticles; inflamation; endothelial

Introduction

The advent of the nanotechnology revolution brings with it a host of new potential health issues that may ensue following exposure to intentionally engineered materials, i.e., those materials that are designed to serve a particular technological function. New metal oxide nanomaterials are being developed for a wide range of novel applications. Nanoscale lanthanide (rare earth) oxides are currently used as catalysts for automobile exhausts. Cerium oxide is used in conjunction with iron for this purpose, serving an enormous market and introducing potential hazards for the environment and human health during manufacture or use. Nanoscale cerium oxide is also a very attractive high-surface-area catalyst for fuel cell applications. Kang and Wang (2003) have shown that it is possible to use cerium, terbium, and praseodymium oxide nanoparticles to produce H_2 for solid oxide fuel cell applications; this is a market that can be expected to grow significantly, leading to

Address for Correspondence: Ian M. Kennedy, Department of Mechanical and Aeronautical Engineering, University of California, Davis, CA 95616, USA. kennedyim@mac.com.

Declaration of interest: The authors report no conflicts of interest. The authors alone are responsible for the content and writing of the paper.

environmental dispersion of these materials as they are used and eventually discarded. Lanthanide oxides are used widely as phosphors for displays; nanoscale oxides of terbium, europium, samarium, etc. find application in solid-state lighting, another potentially huge market. The lanthanide oxides are also useful as nanoparticle labels in biology, providing some benefits over the more widely known quantum dot materials of CdSe and ZnS. As an example, it has been shown that it is possible to carry out highly sensitive immunoassays using Eu and Tb oxide nanoparticles (Feng et al. 2003; Kennedy et al. 2004) for monitoring toxins in the environment.

Zinc oxide (ZnO) and tin oxide (SnO_2) have attracted a great deal of recent interest. These materials are semiconductors that exhibit a range of very useful properties. ZnO exhibits piezoelectric behavior (Zhao et al. 2004), and both ZnO and SnO_2 are used in materials for photo catalysis (Akurati et al. 2005). Tin oxide is also used in transparent and heat reflective coatings for displays and solar cells (Hall et al. 2004). These materials have a conductivity that changes as molecules absorb on their surfaces, so they are used as solid-state gas sensors (Comini et al. 2002; Sahm et al. 2004). New synthesis methods for ZnO and SnO_2 are offering a range of novel morphologies, including nanobelts, nanorings, nanowires, and nanosprings with new functionalities (Comini, Faglia, Sberveglieri, Pan, and Wang 2002; Wang et al. 2004; Wang 2003; Wang 2004a; Wang 2004b). In order to be optimal gas sensors, these materials typically have a very large surface area. Their large surface area may also have an impact on their toxicity when mass is used as a measure of dose.

Iron oxide is a material that is finding new applications in nanotechnology due to its magnetic properties. The two most common forms of iron oxide for magnetic applications are Fe_3O_4 (magnetite) and γ-Fe_2O_3 (maghemite). These oxides of iron are used for magnetic recording media and in ferrofluids (Ozaki 2004). Super-paramagnetism is observed in magnetite particles of size <15 nm; it is a desirable property for several widely discussed biomedical applications, including as a contrast agent for magnetic resonance imaging (Thorek et al. 2006), targeted drug delivery, hyperthermic cancer treatment (Sunderland et al. 2006), and bioassays (Osaka et al. 2006).

Nanomaterials can be produced by a variety of methods: Solution synthesis is perhaps the most common method and provides the greatest control over particle size; gas-phase methods are more amenable to scale-up to larger production rates but typically do not provide the same control over particle size. Commercialization of nanotechnology will require some degree of scale-up to the economics of the marketplace. It is quite possible that some of the gas-phase methods will become more prevalent as time goes on. The large-scale production of nano-materials has, of course, been a major industry for many years. Companies such as Cabot in the United States, for example, have produced very large amounts of fumed silica and titania for many years. The large-scale production of new materials poses unknown potential health risks. In particular, it seems that the greatest risk of exposure is probably in an occupational setting to workers in the nano industry.

The unintentional release of nanoscale metal oxides has taken place for many years. Metal smelters are major stationary point sources of metal oxides. Metal oxide nanoparticles have been emitted by mobile sources such as diesel engines for decades. The presence of metals and their oxides in association with diesel particulate matter is well established. Typically, iron is the most abundant of the transition metals in ambient aerosol. High-temperature combustion processes, including vehicle operation, are likely to be sources of the metal in the ambient aerosol. Huggins et al. (2000) speciated the metals in urban particulate matter and in NIST standard diesel particulate matter. After calcium, iron was the most abundant metal, followed by zinc. The metals may arise from fuels, from lubricating oil, or from engine components. It is clear that engines, especially those with high lubricating oil

consumption or with a low-quality fuel such as bunker fuel, may be a major source of iron, zinc, vanadium, and nickel in the environment in the form of unintentionally manufactured nanoparticles.

The widespread emission of particulate matter by diesel engines has necessitated the implementation of diesel particulate filters (DPF). DPF require periodic regeneration, during which soot particles on the filter are burned off. Nanoparticles of ceria suspended in fuel have been used as a fuel-borne catalyst to lower the regeneration temperature of DPF for light-duty vehicles (Blanchard et al. 2003), which have low exhaust temperatures compared to those of heavy-duty vehicles. Ceria particles associated with soot particles during diesel combustion result in enhanced soot oxidation (Jung et al. 2005). However, there have been concerns about possible adverse health effects of exposure to ceria nanoparticles in the case of DPF failure or malfunction (HEI 2001).

The most likely route of significant exposure to these materials, whether engineered or unintentionally manufactured, is through inhalation. A great deal has been learned over the past few years about the inhalation of ambient ultrafine particles and their translocation to other organs. Less is known about the fate and effects of engineered nanoparticles whose composition may be quite different from some of those that are found in the environment and have been released by mobile or stationary power sources. While it is known that the size of particles is important in determining the sites of their deposition and translocation through the human body, the interaction of particles with cells still raises significant questions, including issues of cell membrane–particle interactions and the role of surface charge and bioavailability, typically determined by the solubility of materials once they enter a cell. Of particular relevance to the present study, ultrafine particles have been shown to cross the pulmonary epithelial barrier into the bloodstream (Kreyling et al. 2002; Nemmar et al. 2002), thereby possibly exposing the vascular endothelium, the monolayer of cells lining the inner surfaces of blood vessels, to particles. The amount that translocates may be quite small, as suggested by Wiebert et al. (2006) in a more recent experiment with radiolabeled carbonaceous particles that were 100 nm in diameter. This experiment took care to control for leaching of the technetium label from the particles. Only 1% or so of the delivered particles or their label were found to be translocated, leaving open the question of the importance to health of this small fraction. Despite this uncertainty, it is worthwhile to examine the response of varied cell types, including aortic endothelial cells, to nanoparticles.

In our earlier study of iron, zinc, and yttrium oxide nanoparticles, we (Gojova et al. 2007) exposed confluent monolayers of human aortic endothelial cells (HAECs) to various concentrations (1 ng/ml to 50 μg/ml) of the oxide nanoparticles in cell culture media for a period of 1 to 8 h. New data obtained by dynamic light scattering have shown that the size of the iron particles, following dispersion by a probe sonicator, asymptoted to about 100 nm hydrodynamic diameter after a few hours in both deionized water and our cell growth medium, indicating reasonable recovery of the mean aerodynamic diameter of about 60 nm that we measured with an SMPS instrument. Sonication with a water bath resulted in an asymptotic size of about 200 to 300 nm in suspension in growth medium.

Following treatment with particles, samples of cells were fixed, sectioned, and examined by transmission electron microscopy (TEM). The results in Figure 1 indicate that the HAECs incorporated the particles of iron and ytrrium oxides with equal success. In both cases, the particles were found within well-defined vesicles in the cells. The Fe_2O_3 particles incorporated in the cells maintained their original morphology with a faceted feature (Figure 2), while the Y_2O_3 particles appeared to have undergone substantial “slaking,” suggesting that they had dissolved to some extent. We also saw significant differences in the ability of these materials to induce inflammatory responses in the cells, as seen by mRNA and protein

levels of specific markers including intercellular adhesion molecule-1 (ICAM-1), interleukin-8 (IL8), and monocyte chemoattreactant protein-1 (MCP-1). Ytrrium and zinc showed clear evidence of inflammation at concentrations of 10 μg/ml or higher, while iron showed none, highlighting the importance of composition, bioavailability, and reactivity of the different metals.

The interiors of many intracellular vesicular structures are acidic. For instance, lysosomes present an environment with pH as low as 4.5 (Asokan and Cho 2002; Reijngoud 1978). Endosomes are also acidic with pH as low as 5 (Helenius et al. 1983). Phagosomes, the organelles involved in phagocytosis, are also acidic, with pH as low as 5 (Schlesinger 1994). It is conceivable that when metal oxide nanoparticles are taken up by a cell and sequestered in vesicles such as lysosomes, endosomes, or phagosomes, dissolution of the nanoparticles may occur, depending on the metal oxide reactivity toward the acidic environment. An intriguing idea is that the intracellular dissolution of the metal oxide particles may induce local or global physiological effects. In the present article, we extend our earlier work on HAECs to include the impact of cerium oxide on cellular inflammation. We also argue that the observed inflammatory responses are consistent with a role for metal oxide dissolution.

Experiments

Ceria particle synthesis

Various techniques such as electrochemical (Garcia-Heras et al. 2004; Ha et al. 2006), hydrothermal (Corradi et al. 2006; Zhang et al. 2006), pyrolysis (Fu et al. 2005; Petrova et al. 2006), and precipitation (Fu, Lin, and Hsu 2005) methods have been used to synthesize CeO_2 particles. Among these methods, the flame synthesis technique has advantages such as high production rates and versatility to make a wide range of particles from a few nanometers to a few hundred nanometers in size. For this study, we synthesized ceria ultrafine particles using the spray flame synthesis technique to extend our earlier work on iron, yttrium, and zinc oxide toxicity and to investigate the inflammatory potential of ceria particles in HAECs.

A spray flame burner as shown in Figure 3 was used to synthesize ceria particles. The spray flame burner was placed in a chamber where there was minute upward flow from the small opening at the bottom of the chamber to the hood above. This helped to stabilize the flame and to prevent possible exposure to researchers during synthesis. Cerium(III) acetate hydrate (Aldrich, >99.9 %) was dissolved in deionized water to make 30 m*M* precursor solution. Liquid precursor was fed into the spray flame at 20 ml/h by a syringe pump. An atomizing gas of 2.0 lpm produced 10- to 20-μm droplets as it passed through the small area annular gap as described in a previous study (Dosev et al. 2006). In all experiments, 1.8 lpm of hydrogen flow was fed and entrained into the mixture of air droplet spray jet to form a hydrogen fueled spray flame. Either 2.0 lpm oxygen or 2.0 lpm nitrogen was used as a co-flow to vary the flame temperature slightly. A four-channel MKS 647C mass flow controller was used to control the gas flows. A cold finger was used to collect ceria particles using thermophoresis. Samples were washed using 100% ethanol and sonicated in a sonic bath for 30 min to break up loose aggregation made during sampling. The Brunauer, Emmett, and Teller (BET) gas absorption method was applied to examine the surface area of the sample. A sampling probe was positioned 8 cm above the tip of the flame for online size distribution measurement using a scanning mobility particle sizer (SMPS), consisting of a TSI 3081 differential mobility analyzer (DMA) and a condensation particles counter (CPC; TSI model 3010). Samples made under nitrogen co-flow condition were used for the inflammation study.

Cell culture and exposure to nanoparticles

Human aortic endothelial cells (HAECs) were incubated for 4 h with different concentrations (0.001–50 μg/ml) of CeO_2 nanoparticles. We subsequently measured mRNA levels of the three inflammatory markers intercellular adhesion molecule 1 (ICAM-1), interleukin (IL)-8, and monocyte chemotactic protein (MCP-1) using quantitative real-time PCR. The details of the procedures can be found in Gojova et al. (2007).

Results and discussion

Particle size distributions (Figure 4) were compared for N_2 co-flow and O_2 co-flow flame conditions, which have different flame temperatures. The particle size distributions and peak diameters (35–40 nm) were very similar in both cases, as measured by SMPS. The XRD results in Figure 5 show broad peaks due to small crystallite sizes. The crystallite sizes were 3 and 6–7 nm for O_2 and N_2 co-flow cases, respectively. The domain sizes were affected by the flame temperature change, and they were much smaller than the mean diameter in the particle size distribution. The XRD results for two different flame temperatures indicated that more than 95% of the samples were CeO_2. We could not find a signature for other cerium oxides such as CeO_3 at the detection limit of XRD. Surface areas determined by BET measurements were 18.5–20.7 m^2/g. Assuming a bulk density of 7.2 g/cc for ceria particles and spherical shape, the equivalent diameter was ~44 nm, which is close to the mean diameter measured by SMPS. is suggests ceria particles might be bigger than the crystal domain size; in other words, we have synthesized polycrystalline ceria particles. We attempted to verify the in situ hydrodynamic particle diameter with dynamic light scattering (DLS) in water and in cell growth medium. We found that it was difficult to obtain reliable measurements with DLS due to two factors: a relatively small refractive index of ceria, and the small primary particle size. While measurements of iron oxide were possible at concentrations as low as 10 μg ml^{-1}, we could not obtain measurements of the ceria particles at our working concentrations. Assuming Rayleigh scattering, it is possible to estimate that the combined reduction in refractive index relative to iron oxide, and a reduction in the mean particle diameter by a factor of 2, combine to reduce the light scattering power by about a factor of 100, leading to the observed difficulty in obtaining reliable DLS data for ceria in situ.

Incubation of HAECs with ceria particles produced modest mRNA upregulation of the inflammatory markers IL8 and MCP-1 (Figure 6). The mRNA increase relative to control was to some extent concentration dependent—the levels were slightly higher at particle concentrations of 50 μg/ml than at 10 μg/ml. More specifically, 10 μg/ml of ceria particles increased IL-8 mRNA levels by 1.4 ± 0.2 times and MCP-1 levels by 1.4 ± 0.4 times in comparison with control cells ($p > .05$); 50-μg/ml samples increased mRNA of the same markers by 1.8 ± 0.5 ($p < .05$) and 2.0 ± 0.6 times ($p > .05$), respectively. No increase was found at the lower concentrations, and there was no significant cell loss at any of the concentrations studied. These results place CeO_2 toward the Fe_2O_3 end of our scale of oxide inflammatory potential.

Assuming that CeO_2 nanoparticles are taken up into HAECs' vesicular pathways in a manner similar to Fe_2O_3, Y_2O_3, and ZnO particles, it is worthwhile to consider possible effects of intracellular solubility. Dissolution of uptaken metal oxide nanoparticles can change the pH value in the cells' vacuoles, as well as cause an abnormally high concentration of the corresponding metal ions. We propose that the change in pH and electrolyte balance may then affect cellular function including activation of inflammatory pathways. Our earlier results (Gojova et al. 2007) on HAECs treated with Fe_2O_3, Y_2O_3 and ZnO particles showed swelling of the vacuoles that is dependent on the type of metal and the dose of nanoparticles, as seen in Figure 1. In the case of high-dose ZnO treatment, the

swelling of the vacuoles is severe and may have contributed to the cell loss we oberved. Osmotically driven fluid flow across the membrane of the vacuole may be responsible for the observed swelling, but the detailed mechanisms remain to be elicidated. Compared to the Y_2O_3 or ZnO particles, the Fe_2O_3 particles caused much less swelling of the vesicles. This may have been a result of the different degrees of intracellular dissolution of the different types of particles as suggested by Figure 2.

The reactivity of a metal oxide nanoparticle towards acid is dependent upon the metal, oxidation state of the metal, and polymorphism of the oxide. As a general rule, the higher the electronegativity of an element, the more acidic is its oxide. Electronegativity of the elements decreases from right to left across the periodic table and decreases down the column. Alkali metals and alkaline earth metals form oxides that react readily with acids; on the other hand, SiO_2 is generally viewed as an acidic oxide. The acidity of transition metal oxides is dependent on both the type of metal and the oxidation state of the metal. ZnO dissolves in both acids and bases (Gerischer and Sorg 1992). Weak acids, such as acetic acid, act as proton donors and complexing agents to accelerate the dissolution. We have carried out some simple laboratory tests on a few metal oxide nanoparticles that have shown that the reactivity toward ascorbic acid (pH 4) and citric acid (pH 5.5) increases in the order of: γ-Fe_2O_3 → cubic Y_2O_3 → cubic Eu_2O_3 → ZnO. Zinc oxide nanoparticles immediately neutralized both ascorbic acid (pH 4) and ascorbate– acetate buffer solution (pH 5.5). On the other hand, γ-Fe_2O_3 was unreactive.

The solubility of nanoparticles, both in water and in cell growth medium, is an important aspect of in vitro experiments. Clearly it is possible for particles to dissolve prior to engaging with cells. In fact, cells may interact with soluble components rather than with nanoparticles themselves, as Franklin (2007) has shown in the case of ZnO in water; the toxicity of the Zn to microalgae was found to be primarily due to dissolved zinc. Franklin (2007) measured the solubility of zinc oxide nanoparticles in water at pH 7.6 with dialysis. Franklin found that dissolution took place over a period of 10 to 40 h or more. This time scale is longer than our typical incubations with cells. Although Zn and Y may be soluble thermodynamically, the kinetics may not be favorable for significant dissolution at neutral pH over the time course of an experiment. At other pH levels, however, dissolution kinetics may be considerably different. This emphasizes the need for detailed assessment of particle dissolution rates within intracellular vesicles.

Nanoparticles can interact with proteins that are in the cell growth medium and that are on cellular surfaces. In this case, the cell may not encounter a pure metal oxide surface but rather a surface that is surrounded by a protein corona as described by Lynch and Dawson (2008). A considerable number of researchers have investigated this issue, often with a viewpoint toward drug delivery and therapeutics (Allen et al. 2006; Cedervall et al. 2007; Lynch and Dawson 2008). Because we are dealing with metal oxide nanoparticles, as opposed to polymeric particles and other materials, we expect that the major interaction with the surface will be through electrostatic (or possibly additional hydrophobic) processes that lead to a physical adsorption. Table 1 provides a list of the pH at the point of zero charge for a variety of oxides. Based on this compilation, we expect that the iron, yttrium, zinc, and cerium oxides will be close to zero or positively charged at pH 7. Silica is exceptional, with a very low pH at its point of zero charge. The other notable positively charged oxides of technological interest are tin and zirconium oxides. Li et al. (2006) showed that the physical adsorption of proteins (in their case, bovine serum albumin [BSA]) to the surfaces of flame-sprayed metal oxide nanoparticles is primarily through an electrostatic interaction. If this is true, then we would not expect significant differences in the interactions of the different forms of metal oxides that we have examined with proteins, possibly leading to similar

uptake for the different oxides. Electron microscope images support this conjecture for the case of iron, ytrrium, and zinc oxides; TEM results were not obtained for cerium oxide.

Our previous BET data (Gojova et al. 2007) indicated that nanoparticle delivery to the HAECs correlated directly with particle concentration in the cell culture medium. Fe_2O_3 nanoparticles failed to provoke an inflammatory response in HAECs at any of the concentrations tested; CeO_2 elicited a weak response, and Y_2O_3 and ZnO nanoparticles elicited a pronounced inflammatory response above a threshold concentration of 10 μg/ml. At the highest concentration, ZnO nanoparticles also led to considerable cell loss.

Although equilibrium calculations, such as MINTEQ, indicate solubility of the metal oxides, it is important to consider the rates of dissolution. If the rates of dissolution are small compared with the rate of uptake into cells, or with the time scale of incubation, then the particles are in effect insoluble. It is possible to estimate the rates of dissolution of several metal oxides of interest at pH typical of lysosomes from data available in the literature. The rate of dissolution of ZnO particles can be estimated from the measured rates that were reported by Gerischer and Sorg (1992) by assuming that the rate of mass dissolution is proportional to the particle surface area,

$$\frac{dm}{dt} = -\pi M \omega d^2 \tag{1}$$

in which m is the mass of the particle, t is time, M is the molecular weight of ZnO (65 g mol^{-1}), ω is the experimental rate of dissolution (2×10^{-7} mol cm^{-2} h^{-1}) reported by Gerischer and Sorg for a pH of about 5, and d is the particle diameter. With a particle density ρ of 5.6 g cm^{-3}, Eq. (1) can be integrated to yield the time for complete dissolution of a particle with initial diameter d_0:

$$t = \frac{d_0 \rho}{2 M \omega} \tag{2}$$

For an initial diameter of 100 nm, Eq. (2) estimates the total time for dissolution to be about 2 h; endocytosis can occur much more quickly, allowing cells to incorporate undissolved particles. The estimated time scale of dissolution of ZnO is consistent with the period of incubation that we have used in our studies, suggesting that it is possible for considerable phase change of ZnO to occur over the times that we have used in our work.

We can consider a similar calculation of the dissolution rate of CeO_2. Tamilmani et al. (2005) measured the reductive dissolution of 300-nm particles of CeO_2 in an ascorbic acid solution over a range of pH. The concentration of dissolved Ce was determined through ICPMS analysis. Analysis of their reported Ce concentrations as a function of time indicates that the dissolution rate of CeO_2 is approximately 4×10^{-9} mol cm^{-2} h^{-1} at pH 6. Complete dissolution of a 100nm particle would take about 400 h, considerably longer than the ZnO particles. The rate of dissolution of iron oxide can be estimated from published data (Martin 2003); it is several orders of magnitude lower than the ceria dissolution rate at pH 5 to 6.

Intact particles can be endocytosed within cells in time scales of the order of minutes. The estimated dissolution rates suggest that it is possible that once inside a cell, oxides like Zn can readily dissolve while iron oxide dissolution rates are so low that negligible amounts of iron are dissolved on the time scale of an incubation, i.e., a few hours. It is possible that a rapid dissolution process may overwhelm the intracellular buffering capacity in HAECs and

may thus contribute to the observed inflammatory response. We submit that it may be useful to consider the impact of dissolution rates of basic or amphoteric oxides on cellular homeostasis.

Conclusions

Flame spray pyrolysis was able generate an aerosol of cerium oxide (CeO_2) with a median diameter of about 40 nm. Human aortic endothelial cells that were exposed to cerium oxide nanoparticles did not exhibit significant inflammatory response as measured by markers such as IL-8, ICAM-1, and MCP-1. is finding can be understood in terms of the rates of dissolution of metal oxides in acidic environments typical of lysosomes. Iron oxide is very insoluble under these conditions, whereas zinc oxide dissolves quite rapidly. Cerium oxide dissolves much slower than zinc oxide. A fast rate of dissolution may overwhelm the cells' natural regulatory mechanisms, triggering an inflammatory response.

Acknowledgments

The authors thank Alexandra Navrotsky, John Neil, and Weiqun Chen for use of XRD and BET instruments and related technical assistance. This work was supported in part by grants from the Superfund Basic Research Program with grant no. 5P42ES04699 from the National Institute of Environmental Health Sciences, National Institutes of Health, P30-ES05705 from NIEHS, and HL55667 from NHLBI. Research described in this article was also conducted under contract to the Health Effects Institute (HEI), an organization jointly funded by the U.S. Environmental Protection Agency (EPA) (Assistance Agreement R82811201) and automotive manufacturers. The contents of this article do not necessarily reflect the views of HEI; nor do they necessarily reflect the views and policies of the U.S. EPA or of motor vehicle and engine manufacturers. Although the research described in the article has been funded in part by the U.S. Environmental Protection Agency through grant RD-83241401-0 to the University of California, Davis, it has not been subject to the agency's required peer and policy review and therefore does not necessarily reflect the views of the agency and no official endorsement should be inferred.

References

Akurati KK, Vital A, Hany R, Bommer B, Graule T, Winterer M. One-step flame synthesis of SnO_2/TiO_2 composite nanoparticles for photocatalytic applications. International Journal of Photoenergy 2005;7:153–161.

Allen LT, Tosetto M, Miller IS, O'Connor DP, Penney SC, Lynch I, Keenan AK, Pennington SR, Dawson KA, Gallagher WM. Surface-induced changes in protein adsorption and implications for cellular phenotypic responses to surface interaction. Biomaterials 2006;27:3096–3108. [PubMed: 16460797]

Asokan A, Cho MJ. Exploitation of intracellular pH gradients in the cellular delivery of macromolecules. Journal of Pharmaceutical Sciences 2002;91:903–913. [PubMed: 11948528]

Blanchard G, Sequelong T, Michelin J, Schuerholz S, Terres F. Ceria-based, fuel-borne catalysts for series diesel particulate filter regeneration. SAE Technical Papers 2003-2001-0378. 2003

Cedervall T, Lynch I, Lindman S, Berggard T, Thulin E, Nilsson H, Dawson KA, Linse S. Understanding the nanoparticle–protein corona using methods to quantify exchange rates and affinities of proteins for nanoparticles. Proceedings of the National Academy of Sciences of the United States of America 2007;104:2050–2055. [PubMed: 17267609]

Comini E, Faglia G, Sberveglieri G, Pan ZW, Wang ZL. Stable and highly sensitive gas sensors based on semiconducting oxide nanobelts. Applied Physics Letters 2002;81:1869–1871.

Corradi AB, Bondioli FB, Ferrari AM, Manfredini T. Synthesis and characterization of nanosized ceria powders by microwave-hydrothermal method. Materials Research Bulletin 2006;41:38–44.

Dosev D, Guo B, Kennedy IM. Photoluminescence of Eu^{3+}: Y_2O_3 as an indication of crystal structure and particle size in nanoparticles synthesized by flame spray pyrolysis. Journal of Aerosol Science 2006;37:402–412.

Feng J, Shan G, Maquieira A, Koivunen M, Guo B, Hammock BD, Kennedy IM. Functionalized rare earth oxide nano particles for use as biomolecular labels. Analytical Chemistry 2003;75:5282–5286.

Franklin NM. Comparative toxicity of nanoparticulate ZnO, bulk ZnO, and $ZnCl_2$ to a freshwater microalga (*Pseudokirchneriella subcapitata*): The importance of particle solubility. Environmental Science & Technology 2007;41:8484–8490. [PubMed: 18200883]

Fu YP, Lin CH, Hsu CS. Preparation of ultrafine CeO_2 powders by microwave-induced combustion and precipitation. Journal of Alloys and Compounds 2005;391:110–114.

Garcia-Heras M, Jimenez-Morales A, Casal B, Galvan JC, Radzki S, Villegas MA. Preparation and electrochemical study of cerium–silica sol–gel thin films. Journal of Alloys and Compounds 2004;380:219–224.

Gerischer H, Sorg N. Chemical dissolution of zinc-oxide crystals in aqueous electrolytes—An analysis of the kinetics. Electrochimica Acta 1992;37:827–835.

Gojova A, Guo B, Kota RS, Rutledge JC, Kennedy IM, Barakat AI. Induction of inflammation in vascular endothelial cells by metal oxide nanoparticles: Effect of particle composition. Environmental Health Perspectives 2007;115:403–409. [PubMed: 17431490]

Ha HW, Yun NJ, Kim MH, Woo MH, Kim K. Enhanced electrochemical and thermal stability of surface-modified $LiCoO_2$ cathode by CeO_2 coating. Electrochimica Acta 2006;51:3297–3302.

Hall DL, Wang AA, Joy KT, Miller TA, Wooldridge NS. Combustion synthesis and characterization of nanocrystalline tin and tin oxide (SnO_x, x=0–2) particles. Journal of the American Ceramic Society 2004;87:2033–2041.

HEI. Communication 9. Evaluation of Human Health risk from cerium Added to diesel Fuel. Health Effects Institute; Boston, MA, USA: 2001.

Helenius A, Mellman I, Wall D, Hubbard A. Endosomes. Trends in Biochemical Sciences 1983;8:245–250.

Huggins FE, Huffman GP, Robertson JD. Speciation of elements in NIST particulate matter SRMs 1648 and 1650. Journal of Hazardous Materials 2000;74:1–23. [PubMed: 10781714]

Jung HJ, Kittelson DB, Zachariah MR. The influence of a cerium additive on ultrafine diesel particle emissions and kinetics of oxidation. Combustion and Flame 2005;142:276–288.

Kang Z, Wang ZL. Novel oxides for cycled hydrogen production from methane and water using a temperature swing. Advanced Materials 2003;15:521–526.

Kennedy, IM.; Koivunen, M.; Gee, S.; Cummins, CM.; Perron, R.; Dosev, D.; Hammock, BD. Nanoscale fluoro-immunoassays with lanthanide oxide nanoparticles. In: Islam, M.; Dutta, AK., editors. Proc SPIE. Vol. 5593. 2004. p. 329-339.

Kosmulski, M. Chemical Properties of Material Surfaces. Vol. 102. New York: Marcel Dekker; 2001.

Kreyling WG, Semmler M, Erbe F, Mayer P, Takenaka S, Schulz H, Oberdorster G, Ziesenis A. Translocation of ultrafine insoluble iridium particles from lung epithelium to extrapulmonary organs is size dependent but very low. Journal of Toxicology and Environmental Health A 2002;65:1513–1530.

Li D, Teoh WY, Selomulya C, Woodward RC, Amal R, Rosche B. Flame-sprayed superparamagnetic bare and silica-coated maghemite nanoparticles: Synthesis, characterization, and protein adsorption–desorption. Chemistry of Materials 2006;18:6403–6413.

Lynch I, Dawson KA. Protein–nanoparticle interactions. Nano Today 2008;3:43–47.

Martin, ST. Precipitation and dissolution of iron and manganese oxides. In: Grassian, V., editor. Environmental Catalysis. Taylor and Francis; Boca Raton: 2003. p. 61-82.

Nemmar A, Hoet PH, Vanquickenborne B, Dinsdale D, Thomeer M, Hoylaerts MF, Vanbilloen H, Mortelmans L, Nemery B. Passage of inhaled particles into the blood circulation in humans. Circulation 2002;105:411–414. [PubMed: 11815420]

Osaka T, Matsunaga T, Nakanishi T, Arakaki A, Niwa D, Iida H. Synthesis of magnetic nanoparticles and their application to bioassays. Analytical and Bioanalytical Chemistry 2006;384:593–600. [PubMed: 16402174]

Ozaki M. Magnetic particles: Preparation, properties, and applications. Surface and Colloid Science 2004;17:1–26.

Petrova NL, Todorovska RV, Todorovsky DS. Spray-pyrolysis deposition of CeO_2 thin films using citric or tartaric complexes as starting materials. Solid State Ionics 2006;177:613–621.

Reijngoud DJ. pH and transport of protons in lysosomes. Trends in Biochemical Sciences 1978;3:178–180.

Sahm T, Madler L, Gurlo A, Barsan N, Pratsinis SE, Weimar U. Flame spray synthesis of tin dioxide nanoparticles for gas sensing. Sensors and Actuators B—Chemical 2004;98:148–153.

Schlesinger, PH. Methods in Cell Biology. Vol. 45. Academic press; NY: 1994. Measuring the pH of pathogen-containing phagosomes; p. 289-311.

Sunderland CJ, Steiert M, Talmadge JE, Derfus AM, Barry SE. Targeted nanoparticles for detecting and treating cancer. Drug Development and Research 2006;67:70–93.

Tamilmani S, Lowalekar V, Raghavan S, Small R. Dissolution characteristics of ceria in ascorbic acid solutions with implications to cleaning. Ultra Clean Processing of Silicon Surfaces VII 2005;103–104:283–286.

Thorek DLJ, Chen A, Czupryna J, Tsourkas A. Superparamagnetic iron oxide nanoparticle probes for molecular imaging. Annals of Biomedical Engineering 2006;34:23–38. [PubMed: 16496086]

Wang XD, Ding Y, Summers CJ, Wang ZL. Large-scale synthesis of six-nanometer-wide ZnO nanobelts. Journal of Physical Chemistry B 2004;108:8773–8777.

Wang ZL. Nanobelts, nanowires, and nanodiskettes of semiconducting oxides—From materials to nanodevices. Advanced Materials 2003;15:432–436.

Wang ZL. Functional oxide nanobelts: Materials, properties and potential applications in nanosystems and biotechnology. Annual Review of Physical Chemistry 2004a;55:159–196.

Wang ZL. Zinc oxide nanostructures: Growth, properties and applications. Journal of the Physics: Condensed Matter 2004b;16:R829–R858.

Wiebert P, Sanchez-Crespo A, Seitz J, Falk R, Philipson K, Kreyling WG, Möller W, Sommerer K, Larsson S, Svartengren M. Negligible clearance of ultrafine particles retained in healthy and affected human lungs. European Respiration Journal 2006;28:286–290.

Zhang YL, Kang ZT, Dong J, Abernathy H, Liu ML. Self-assembly of cerium compound nanopetals via a hydrothermal process: Synthesis, formation mechanism and properties. Journal of Solid State Chemistry 2006;179:1733–1738.

Zhao MH, Wang ZL, Mao SX. Piezoelectric characterization of individual zinc oxide nanobelt probed by piezoresponse force microscope. Nano Letters 2004;4:587–590.

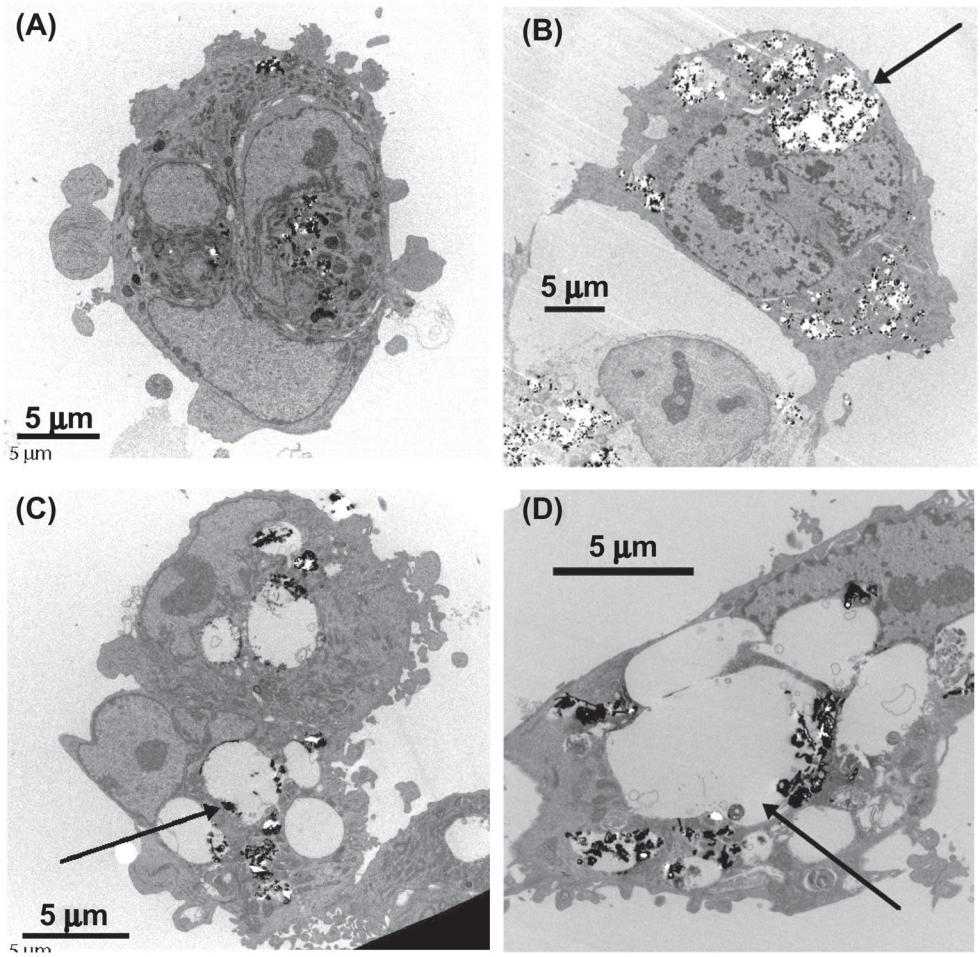

Figure 1.

Human aortic endothelial cells incorporating metal oxide nanoparticles: (a) cells treated with 10 µg/ml Fe_2O_3 particles; (b) cells treated with 50 µg/ml Fe_2O_3 particles; (c) cells treated with 10 µg/ml Y_2O_3 particles; (d) cells treated with 50 µg/ml Y_2O_3 particles. Metal oxide particles are shown as high-density spots. Arrows point to significantly enlarged cell structures. At the same dose, Y_2O_3 particles apparently caused much greater vesicle volume increase.

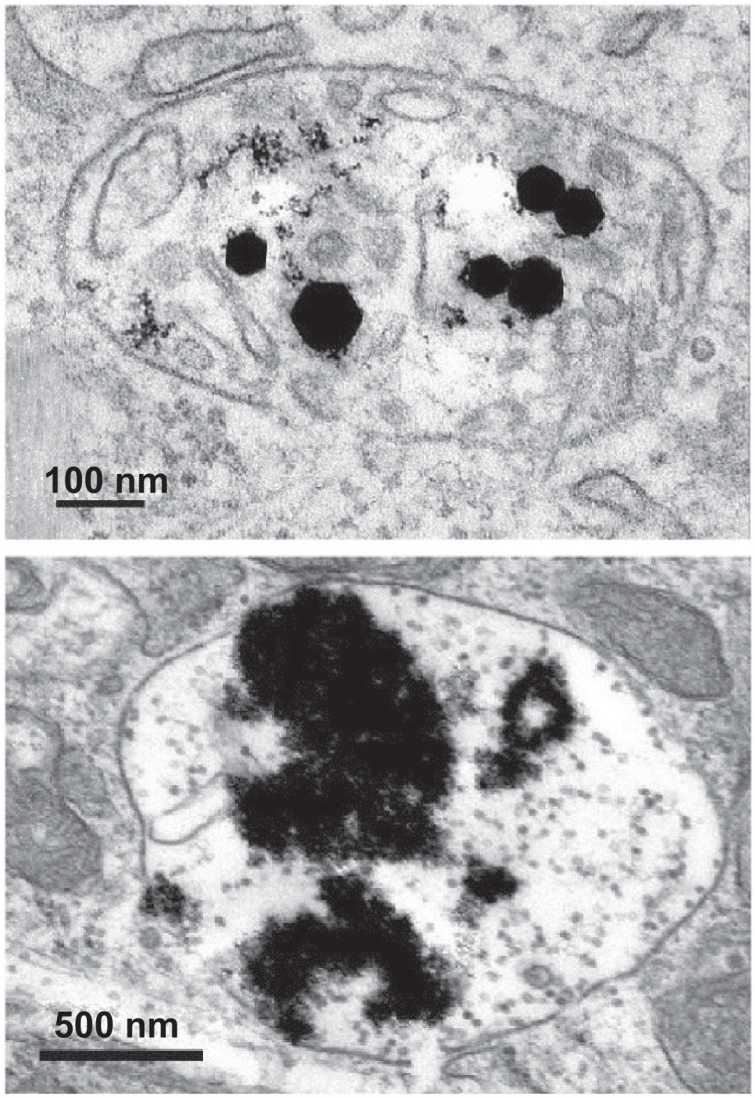

Figure 2.
Fe_2O_3 and Y_2O_3 nanoparticles incorporated in human aortic endothelial cells. Parts in images with highest density are metal oxide particles. Top: Faceted γ-Fe_2O_3 particles indicate little dissolution. Bottom: Sludge-like Y_2O_3 particles suggest significant dissolution.

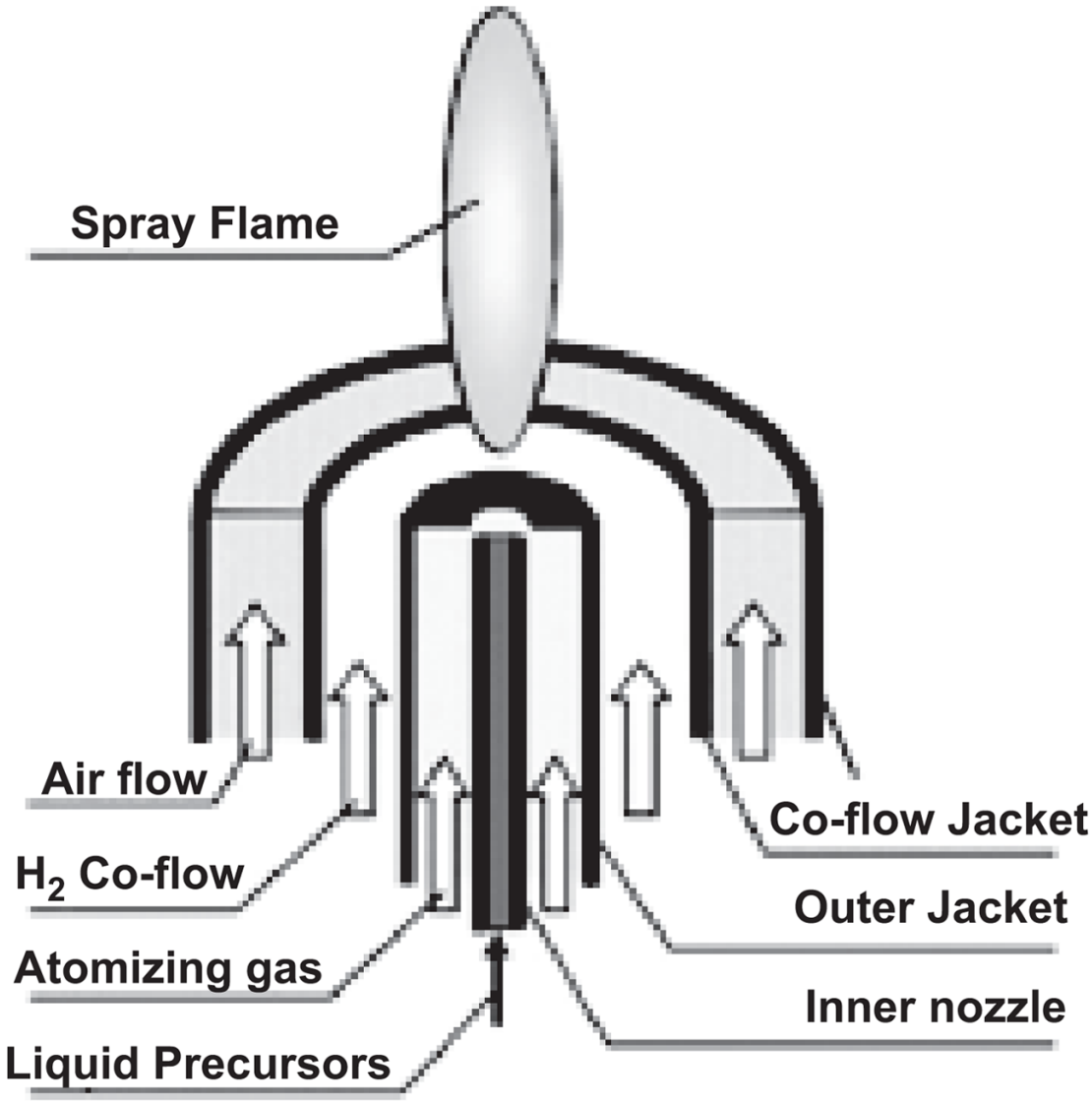

Figure 3.
Schematic of spray flame burner. (See colour version of this figure online at www.informapharmascience.com/iht)

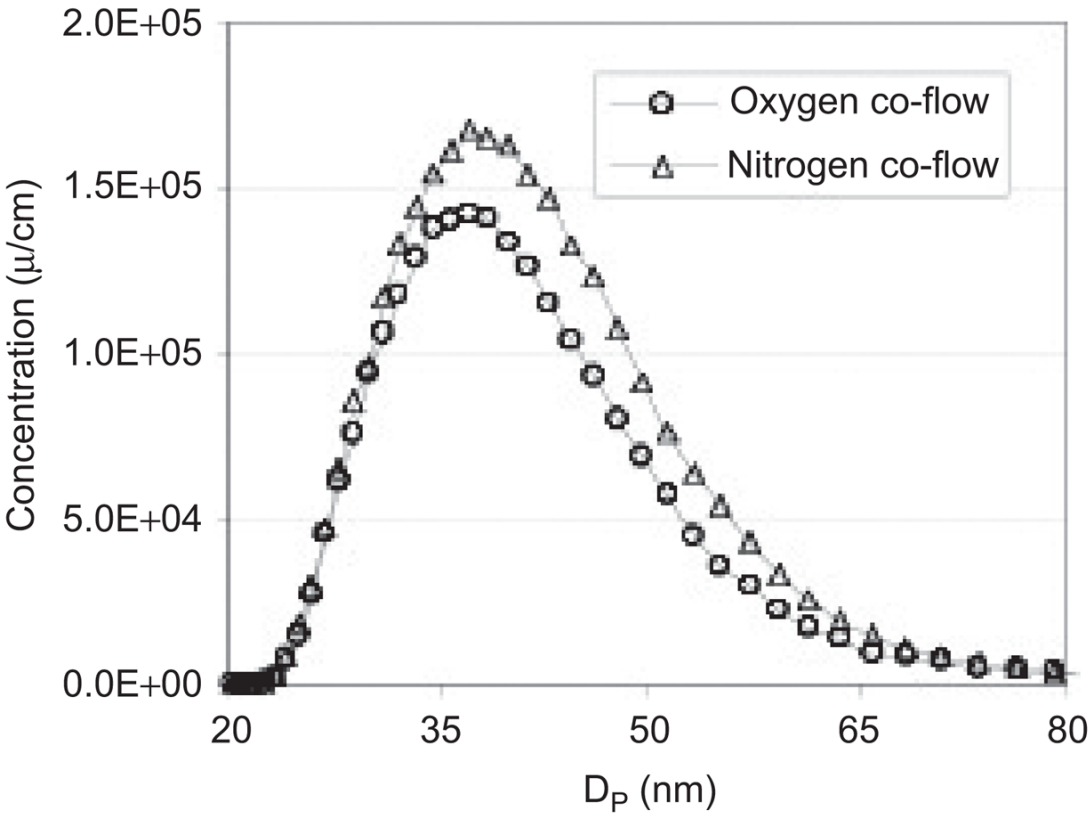

Figure 4.
Particle size distribution for hydrogen fueled spray flame with 30 m*M* cerium acetate hydrate as a precursor solution with O_2 and N_2 co-flows.

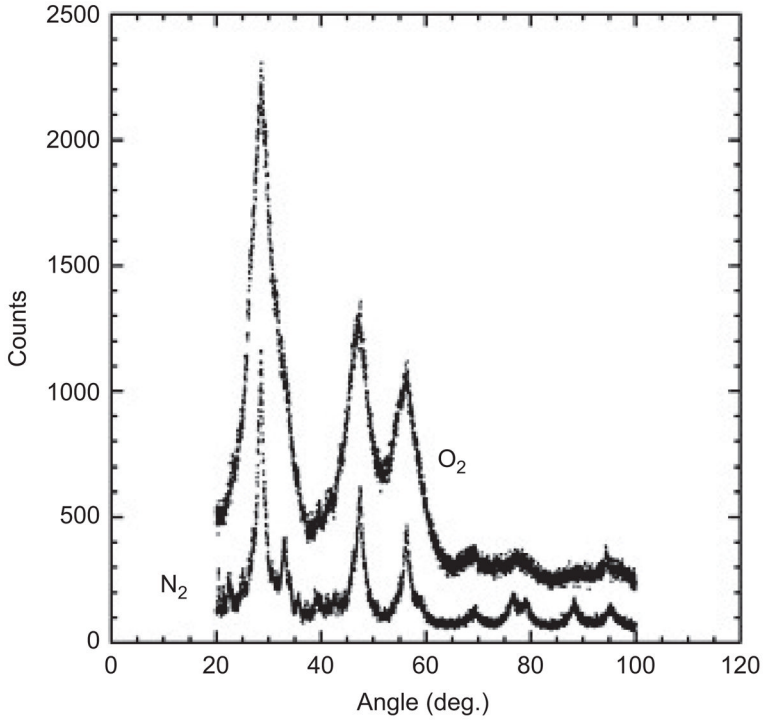

Figure 5.
XRD patterns of ceria particles with O_2 and N_2 co-flows.

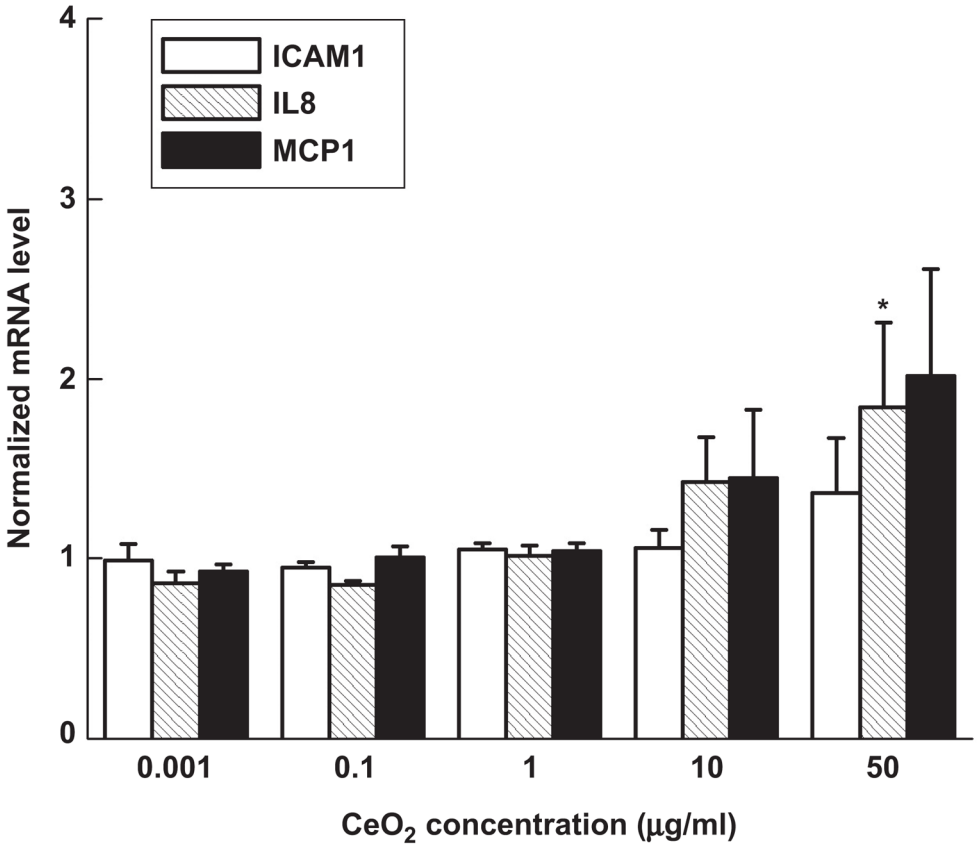

Figure 6.

mRNA levels of the three inflammatory markers ICAM-1, IL-8, and MCP-1 in human aortic endothelial cells incubated for 4 h with ceria particles. Each mRNA value was normalized to the corresponding GAPDH value. Ratios relative to control cells (no particles) are shown. Data are mean ± SEM from three independent experiments run in duplicates. Asterisk denotes statistically significant mRNA level increase relative to control cells ($p < .05$).

Table 1

pH at point of zero charge for various oxides, tabulated by Kosmulski (2001).

	pH
Al_2O_3 (fumed)	9.8
CeO_2	5.2–8.6
CuO	7.5–9.4
Fe_3O_4 (natural)	9.9
Fe_2O_3 (hematite)	7.3–9.5
Fe_2O_3 (maghemite)	5.5
SiO_2 (flame hydrolysis)	3.5
SnO_2	4.2
TiO_2	5.9–7.5
Y_2O_3	7.6
ZnO	8.8–9.8
ZrO_2	4.2–4.5